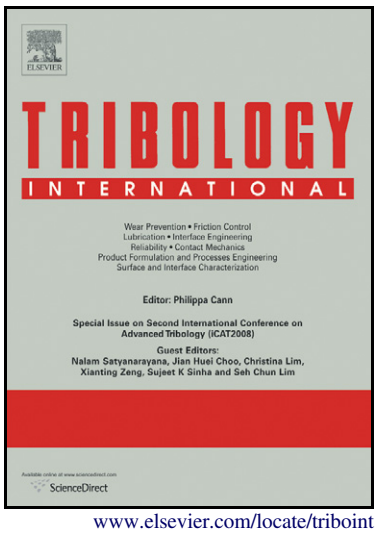

www.elsevier.com/locate/triboint

A comparative study of wear laws for soft-on-hard hip implants using a mathematical wear model

L. Mattei, F. Di Puccio, E. Ciulli

PII: S0301-679X(12)00092-8
DOI: doi:10.1016/j.triboint.2012.03.002
Reference: JTRI2705

To appear in: *Tribology International*

Received date: 24 October 2011
Revised date: 22 February 2012
Accepted date: 7 March 2012

Cite this article as: L. Mattei, F. Di Puccio and E. Ciulli, A comparative study of wear laws for soft-on-hard hip implants using a mathematical wear model, *Tribology International,* doi:10.1016/j.triboint.2012.03.002

A comparative study of wear laws for soft-on-hard hip implants using a mathematical wear model

L. Mattei[a,*], F. Di Puccio[a], E. Ciulli[a]

[a]*Department of Mechanical, Nuclear and Production Engineering, Largo Lucio Lazzarino, 1, Pisa , 56122, Italy*

Abstract

Wear of UHMWPE acetabular components is the most serious threat to the long-term success of hip replacements. Consequently numerical and experimental wear simulations are of great interest. The present study proposes a mathematical wear model and compares the most recent wear laws, based on the so-called cross-shear (CS) effect. Simulations highlighted the variability of wear predictions with the wear factors/laws. Moreover a sensitivity analysis underlined that the kinematic conditions affect volumetric/linear wear more than the loading ones. This study confirms the importance of the CS in wear predictions even if some critical issues are still open, requiring further investigations.

Keywords: hip replacement, wear prediction, cross-shear, wear model

1. Introduction

Wear of conventional Ultra High Molecular Weight Polyethylene (UHMWPE) has historically been recognized as the primary cause of soft-on-hard (SoH) hip implant failure and revision. Attested studies have demonstrated that around 100 millions of submicron UHMWPE particles are released into the periprosthetic fluid for a daily patient activity [1]. This wear debris typically triggers a cascade of adverse tissue reactions leading to osteolysis and implant loosening [2].

In the last decades this limitation has been motivating reseachers in investigating wear mechanisms of UHMWPE, mainly by means of experimental tests. Among these, clinical and laboratory studies can be distinguished. The former are based on *in-vivo* estimation of linear wear by radiography [3, 4] or stereo-photogrammetry [5], or on *in-vitro* wear assessment of retrieved components [6–10]. As far as laboratory studies is concerned, hip joint simulators are being continuously improved for replicating realistic loading and kinematic conditions, e.g. [11, 12]. Pre-clinical experimental wear predictions are certainly a useful and necessary step in the optimization of the design process of Total Hip Replacement (THR), but they can be highly time/cost demanding and allow mainly short-term wear predictions.

In order to bypass these drawbacks, theoretical and numerical approaches can be adopted. Several computational wear models of THRs can be found in the literature, as reviewed in [13], which allow long term wear predictions. The first successful wear simulation of MoP implants was pioneered by Maxian et al. in 1996 [14] and was based on the Archard wear law. Since then, numerical simulations have been carried out to investigate the influence on wear of some design factors such as head size and cup thickness [15, 16], metal backing [17], surface roughness [16, 18], friction coefficient [18] and body weight [16].

Recent understandings of the wear mechanisms of UHMWPE made a break-through towards an improved THR wear modelling possible. It was demonstrated by Wang et al. [19] and by Turell et al. [20] that the UHMWPE-metal wear is strongly affected by multi-directional sliding, known as the Cross-Shear (CS) effect. In addition, other studies, such as [21, 22], showed the effect of the contact pressure on the wear factor. More recently, these findings were introduced in the Archard wear law by defining the wear factor as a function of the so-called cross-shear ratio (CS_r) or both of the CS_r and the local contact pressure, as reported by Kang et al. in [23] and [24], respectively. In addition, experimental works carried out by Wang [25] showed the elastic nature of the deformation of UHMWPE micro-asperities under contact, yielding to a weak validity of the Archard wear law for MoP implants. Consequently a new wear law was presented by Liu et al. [26] and applied to MoP hip replacements, thus obtaining wear predictions in improved agreement with experimental data.

It is worth noting that most of the wear simulations mentioned above, were carried out using commercial Finite Element (FE) codes, integrated with user-defined subroutines by means of a procedure that can be quite complex and computationally expensive. Only rarely an analytical approach was pursued, such as by Raimondi et al. [16], whose model for MoP implants was based on Hertzian pressure distribution and a simplified expression of the sliding distance.

In the current study a mathematical parametric model for SoH hip implants is presented, improved with respect to the one described in [16] in several aspects, such as the contact analysis

*Corresponding author

Email addresses: l.mattei@ing.unipi.it (L. Mattei), dipuccio@ing.unipi.it (F. Di Puccio), ciulli@ing.unipi.it (E. Ciulli)

and the sliding distance evaluation. The main aim of the paper is to compare, by means of the developed model, the most recent wear laws for UHMWPE in terms of volumetric/linear wear predictions. Indeed such wear laws were generally implemented in models with different characteristics (e.g. geometries, material properties or kinematic/loading conditions), so their results are not easily comparable. The sensitivity of such wear laws to different kinematic and loading conditions is also discussed.

2. Wear laws for soft-on-hard hip implants

Wear modelling of SoH implants still remains an open issue and needs both the assumption of simplifying hypotheses and experimental findings.

Generally it is assumed that the wear is localized in the plastic cup, softer than the metallic head. Moreover the surfaces are considered in dry contact, the lubrication effect being taken into account in the wear factor empirically derived. In addition, although several wear mechanisms can affect the implant during *in-vivo* functioning (e.g. fatigue, corrosive wear), only adhesion and abrasion are considered [27]. Under this last hypothesis the Archard wear law holds, stating that, for a translating body, there is a proportionality, through a wear factor k_f, between the volumetric wear V and the product of the resultant normal load L_N and the sliding distance s

$$V = k_f \; L_N \; s \tag{1}$$

Often the Archard wear law is more conveniently written in a local instantaneous form yielding the linear wear rate $h_r(P,t)$ at a point P of the cup surface at a time t

$$h_r(P,t) = k_f(P,t) \; p(P,t) \; |\boldsymbol{v}(P,t)| \tag{2}$$

where $p(P,t)$ is the instantaneous contact pressure and $\boldsymbol{v}(P,t)$ the sliding velocity.

The wear factor is evaluated experimentally by means of pin-on-disk/plate or hip joints simulator wear tests and depends on several factors such as coupled materials, surface roughness, lubrication conditions, hence on the experimental set-up as well. A constant wear factor was used in the first wear simulations by Maxian et al. [14, 15], based on data from [28]. Raimondi et al. [16] considered k_f function of the head roughness R_a, according to results reported in [29].

In the last fifteen years, experimental observations on the UHMWPE wear, e.g. [19], stressed that when polyethylene is subjected to multi-directional sliding against a metallic counter face, the polymeric chains acquire a principal molecular orientation (PMO) in whose direction the surface results harder and the wear resistance increases. On the opposite, in the direction perpendicular to the PMO, i.e. the CS direction, there is a strain softening phenomenon which is predominantly responsible for the detachment of fibrous wear debris from the worn surfaces. The concept is schematically represented in Fig. 1.

In this paper the cross-shear ratio $CS_r(P)$ is defined, in agreement with other studies in the literature [30, 23, 24, 26], as the

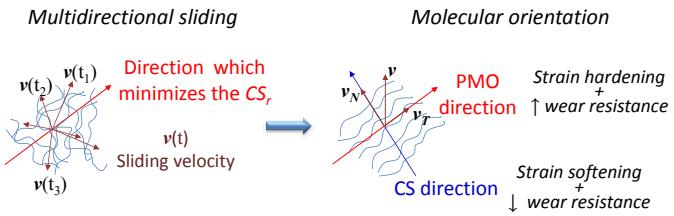

Figure 1: Schematic representation of the cross-shear effect. UHMWPE polymeric chains, initially randomly oriented (a), re-orient in the PMO direction because of multi-directional sliding on a harder counterface (b).

ratio between the frictional work released perpendicularly to the PMO ($W_\perp$) and the total frictional work (W_{tot}) in a load cycle of time period T, that is

$$CS_r(P) = W_\perp(P)/W_{tot}(P) \tag{3}$$

with

$$W_\perp(P) = \int_0^T f(P,t)p(P,t)\,|\boldsymbol{v}(P,t)|\sin^2\zeta(P,t)dt \tag{4}$$

$$W_{tot}(P) = \int_0^T f(P,t)p(P,t)\,|\boldsymbol{v}(P,t)|\,dt \tag{5}$$

Such a definition gives the so called cycle-averaged CS. In the above equations $f(P,t)$ is the friction coefficient, which can vary in place and in time, and $\zeta(P,t)$ is the angle between $\boldsymbol{v}(P,t)$ and the PMO (of unit vector $\boldsymbol{\mu}(P)$), that is

$$\cos\zeta(P,t) = \frac{\boldsymbol{\mu}(P)\cdot\boldsymbol{v}(P,t)}{|\boldsymbol{v}(P,t)|} \tag{6}$$

However, the PMO direction and therefore $\zeta(P,t)$ are not known *a priori*, but they require the solution of an optimization problem, being $\boldsymbol{\mu}(P)$ the direction which minimizes $CS_r(P)$ or, alternatively, $W_\perp(P)$.

As it is commonly assumed that $f(P,t)$ does not vary within a cycle, i.e. $f(P,t) \approx f(P)$, Eq. 3 can be simplified yielding a constant friction cross-shear ratio CS_f:

$$CS_f(P) = \frac{\int_0^T p(P,t)\,|\boldsymbol{v}(P,t)|\sin^2(\zeta(P,t))dt}{\int_0^T p(P,t)\,|\boldsymbol{v}(P,t)|\,dt} \tag{7}$$

Furthermore in the literature, e.g. [30, 23], another simplifying hypothesis is commonly adopted, that is the replacement of the instantaneous pressure with its average value $\bar{p}(P)$ over a load cycle. This leads to the following version of the CS ratio, denoted CS_s, commonly employed in the literature

$$CS_s(P) = \frac{\int_0^T |\boldsymbol{v}(P,t)|\sin^2(\zeta(P,t))dt}{\int_0^T |\boldsymbol{v}(P,t)|\,dt} \tag{8}$$

It is worth noting that CS_s depends only on the kinematic conditions and ranges between 0 and 0.5, the former corresponding to a unidirectional sliding while the latter to circular/squared tracks or whenever $W_\perp = W_\parallel$. $W_\parallel$ is work released in the direction parallel to the PMO; it is also $W_{tot} = W_\perp + W_\parallel$.

Such a quantification of the CS effect enabled Kang et al. [23] to introduce a more complex expression of the wear factor

$$k_f(CS_s) = 3.28\,10^{-7}\ln(CS_s) + 1.62\,10^{-6} \tag{9}$$

As in the above equation, in the following the dependence on the point P will be omitted for brevity, but it should be reminded that the wear factor is function of the cup point through the CS ratios, i.e. $k_f(CS_s(P))$.

Barbour et al. [21] and Wang et al. [22] evidenced that the wear factor of SoH hip implants depends also on the contact pressure. Hence, in 2009, Kang and her research group revised Eq. 9 and proposed a wear factor function of both CS_s and $\bar{p}$ [24]

$$k_f(CS_s, \bar{p}) = \exp\left[13.1 + 0.9\ln(CS_s) - 0.29\,\bar{p}\right] \tag{10}$$

Experimental tests showed that, rather counter intuitively, the wear rate decreases as the average contact pressure increases. This can be explained considering the nature of deformation of the plastic cup. Indeed Wang [25] demonstrated that even if the local contact stresses interesting the PE asperities were higher than the nominal ones, the polymer deformation remained mainly elastic. Therefore the hypothesis of surface plastic deformation, hence the linear relation between the load and the real contact area at the basis of the Archard wear law, was no longer valid. Moving from this observation, a new formulation of the wear law for SoH contacts has been recently proposed by Liu et al. [26]. It proportionally relates the volumetric wear to the product of the nominal contact area A and the sliding distance, according to the following equation

$$V = k_c\,A\,s \tag{11}$$

where k_c is a dimensionless proportionality constant known as wear coefficient. The local instantaneous form of Eq. 11 becomes

$$h_r(P,t) = k_c(P,t)\;|\boldsymbol{v}(P,t)| \tag{12}$$

Also k_c depends on the cross-shear ratio; the expression of k_c proposed by Liu et al. [26], i.e.

$$k_c(CS_s) = \begin{cases} (32\,CS_s + 0.3)\,10^{-9} & 0 \le CS_s \le 0.04 \\ (1.9\,CS_s + 1.6)\,10^{-9} & 0.04 \le CS_s \le 0.5 \end{cases} \tag{13}$$

was obtained from the k_f defined in [30]. It is worth underlying that k_c is assumed to be almost constant with the contact pressure.

All the above mentioned wear laws and wear factor/coefficient expressions are collected in Table 1 together with the references in which they were exploited and defined. The graphical representations of the k_f and k_c expressions are shown in Fig. 2 to better clarify the dependence of such functions on the CS_s.

3. Wear prediction model

An analytical and parametric wear predictive model was developed by the authors for SoH hip implants. The software

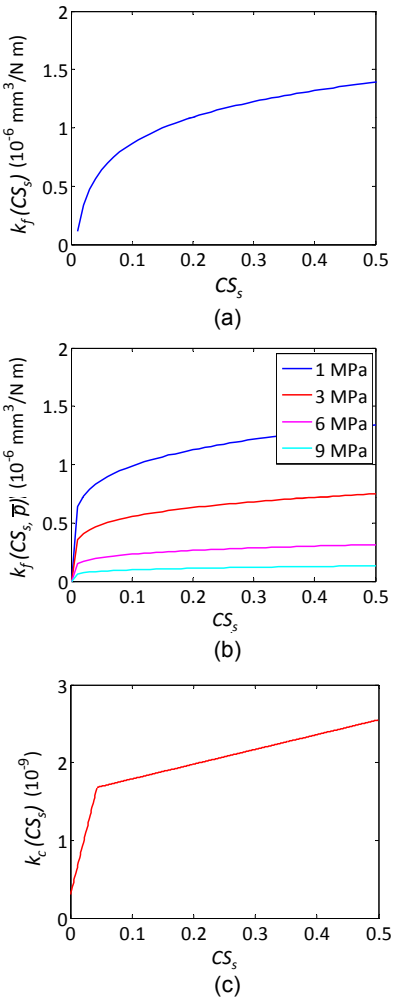

Figure 2: Trends of the wear factor and wear coefficient vs. CS_s according to Kang et al. [23] (a), Kang et al. [24] (b), Liu et al. [26] (c).

Mathematica® was chosen for implementation as it is a very powerful tool for symbolic calculus.

The model was formulated for a left hip implant, characterized by a plastic cup coupled with a metallic or ceramic head, as represented in Fig. 3-a.

3.1. Basic assumptions

The wear model was based on some hypotheses largely adopted in the literature and reported in Sec. 2. The following additional assumptions were made with the aim of simplifying the model and reducing the computational cost:

1. the geometrical variation of the plastic surface due to wear does not affect the contact mechanics;
2. the contribution of the elastic deformation of the cup to the sliding velocity can be disregarded;
3. the contact is considered frictionless;
4. the creep effects are neglected.

Particular attention has to be given to the first hypothesis that can be considered valid if the wear model is used for a comparative analysis of the wear laws and not for corroborating experimental findings.

Wear model				Wear Test		
Wear law	**k_f / k_c**	**k_f / k_c expression**	**Ref.**	**Type**	**Notes**	**Ref.**
$k_f\, L_N\, s$	k_f cost	1.066	Maxian et al. 1996 [14,15]	PoD	--	Streicher et al. 1991 [28]
	$k_f(R_a)$	$8.68\ 10^{-6}\ R_a + 1.51\ 10^{-6}$	Raimondi et al. 2001 [16]	HS	R_a (μm)	Wang et al. 1998 [29]
	$k_f(CS_s)$	$3.28\ 10^{-7}\ \ln(CS_s) + 1.62\ 10^{-6}$	Kang et al. 2008 [23]	MD-PoP	Evaluated at 1 MPa	Kang et al. 2008 [23]
	$k_f(CS_s, \bar{p})$	$\exp(-13.1 + 0.19\ln(CS_s) - 0.29\,\bar{p})$	Kang et al. 2009 [24]	MD-PoP	--	Kang et al. 2009 [24]
$k_c\, A\, s$	$k_c(CS_s)$	$\begin{cases}(32\,CS_s + 0.3)10^{-9} & CS_s \le 0.04\\ (1.9\,CS_s + 1.6)10^{-9} & 0.04 < CS_s \le 0.5\end{cases}$	Liu et al. 2011 [26]	MD-PoP	Calculated as $k_f(CS_s)\,\bar{p}$ with k_f evaluated at 3.18 MPa	Kang et al. 2008 [30]

Table 1: Analytical expressions of wear factors/coefficient. Legend: PoD - Pin on Disk wear test, HS - Hip Simulator wear test, MD-PoP - Multi Directional Pin on Plate.

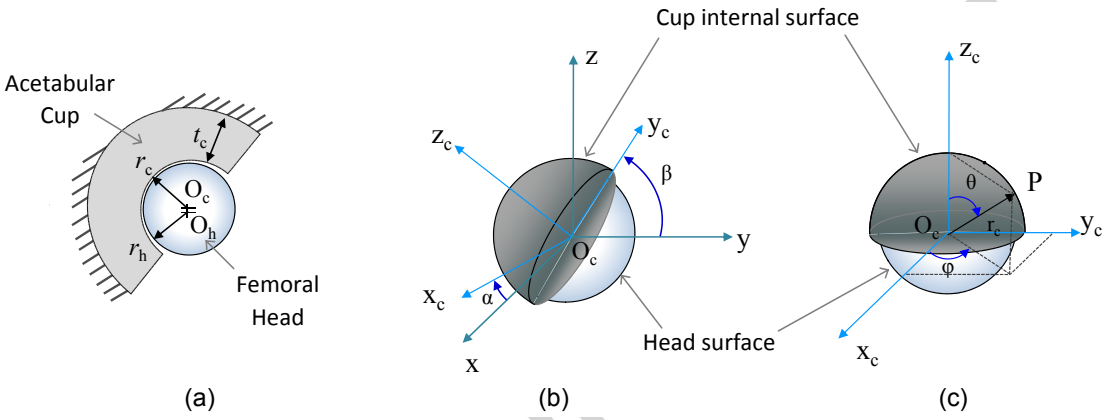

Figure 3: Geometrical characteristics of the model (a). Coordinate reference frames used for model implementation: $C_g = \{O_c, x, y, z\}$ cartesian fixed frame oriented along the anatomical directions (z vertical, x anterior) and $C_c = \{O_c, x_c, y_c, z_c\}$ cartesian frame fixed to the cup (b,c).

As the friction coefficient is very low (i.e. ≤0.065 [31]), the assumption of a frictionless contact was introduced, as in [16], because it implies that the reaction force between the head and the cup lies in the direction joining their centers and this allows an immediate identification of the theoretical contact point. Moreover the variation of the contact actions can be considered negligible. The creep effect was disregarded as not meaningful to the aim of this study, that is the comparison of the wear models. In fact, according to Willing and Kim [32] and Abdelgaied et al. [33], the creep term depends on the material, on the average pressure, on the thickness and on time. As geometry is not updated, cup thickness and pressure distributions remain the same for all the implemented wear models. Therefore considering the creep effect would mean to introduce the same additional term to the different wear depths and thus it was preferred to compare the latter directly. However, according to Abdelgaied et al. [33], the creep contributes for about 5% to the cup thickness reduction.

3.2. Model input

3.2.1. Geometry and materials

The geometry of the implant was characterized by head and cup radii, r_h and r_c respectively, and by the cup thickness t_c (Fig. 3-a). The position of the cup in the pelvic bone was specified by the anteversion (α) and the inclination (β) angles (Fig. 3-b). Two coordinate systems were introduced, described in Figs. 3-b,c: the cartesian fixed global frame $C_g = \{O_c, x, y, z\}$ (with z in the vertical direction, x in the antero-posterior direction) and the cartesian fixed cup frame $C_c = \{O_c, x_c, y_c, z_c\}$.

The geometrical characteristics and the material properties of SoH simulated implant are summarized in Table 2.

3.2.2. Boundary conditions

The cup was considered to be fixed in the pelvic bone and the relative motion assigned to the head. Consequently, the boundary conditions (BCs) consisted in the load applied to the head and the head angular velocity, both conveniently expressed in the reference frame C_g. In this study the wear caused by walking was investigated, thus the loading and the kinematic conditions of the gait cycle were implemented according to liter-

Geometry	
r_c (mm)	14
cl=r_c-r_h (mm)	0.08
t_c (mm)	8
R_a (µm)	0.02
α (°)	0
β (°)	35–45

Material			
Cup	UHMWPE	E_c (GPa)	0.5
		ν_c	0.4
Head	CoCr	E_h (GPa)	210
		ν_h	0.3

Table 2: Geometrical and material data of the simulated SoH hip implant. E and ν are the Young modulus and the Poisson ratio for head and cup material, subscripts h/c respectively.

ature data. In particular data measured *in-vivo* by Bergmann et al. [34] and the BCs applied in Leeds ProSim hip simulator [23, 26] were simulated, as reported in Figs. 4-a,b and Figs. 4-c,d respectively.

3.3. Wear evaluation

Both the Archard wear law and the new wear law were implemented in the local instantaneous forms, Eq. 2 and Eq. 12, respectively. All the expressions of k_f and k_c reported in Table 1 were taken into account. It is worth noting that the simplified cross-shear ratio CS_s, defined in Eq. 8, was employed.

The wear simulation went through three steps concerning the evaluation of the contact pressure, of the sliding distance and of the wear factor/coefficient. The latter, in particular the calculation of $CS_s(P)$, resulted the most critical point of the model, because it required the solution of the minimization problem that can be computationally expensive.

3.3.1. Contact analysis

Contact analysis was a fundamental part of the wear model for evaluating the contact area and the contact pressure. Usually analytical models, e.g. in Raimondi et al. [16], are based on the Herztian theory, although it is hardly applicable in case of conformal geometry and of SoH bearings.

In this study the contact mechanics was solved by means of FE analyses and results fitted in order to be included in Mathematica® as continuous functions.

FE analyses

A simple axial-symmetric FE model was developed in Ansys®, in parametric form for simulating several geometries and load levels. The external side of the cup was considered fixed and the load applied to head as a pressure distributed on its midside surface. A frictionless contact pair was defined between the external surface of the head and the inner surface of the cup. Static analyses were performed increasing the load from zero up to 3000 N in steps of 100 N. A mesh sensitivity analysis was carried out to define the contact element size (1 element/1° angle at the head center), which gave a variation on the maximum pressure below 0.2% with respect to a further mesh refinement (1 element/0.75°).

Fitting of FE results

By fitting the FE results (for a given hip implant), an analytical correlation was established between pressure distribution and two contact parameters, the maximum contact pressure

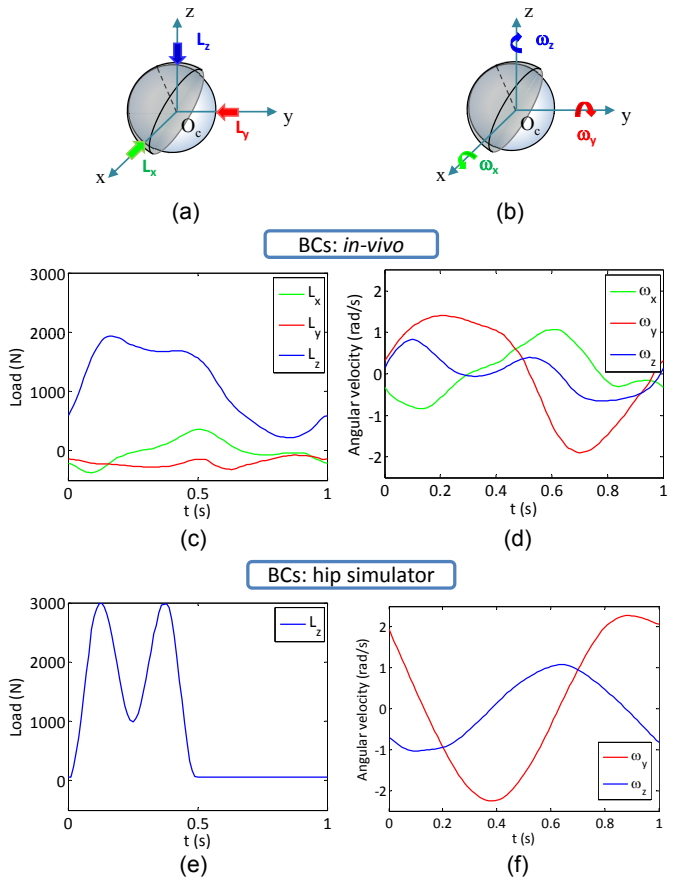

Figure 4: Load (a) and angular velocity (b) components in the fixed anatomical frame C_g. Boundary conditions: loading and kinematic conditions of the gait according to Bergmann et al. [34] (c,d) and Leeds ProSim hip simulator (e,f).

p_{max} and the semi-angular contact width ψ_{max} (Fig. 6-a)

$$p(\psi) = p_{max}\left[1 - \left(\frac{\sin\psi}{\sin\psi_{max}}\right)^2\right]^c \tag{14}$$

where ψ is the angle between the loading direction and the radius of a point P of the cup surface, and c is the power law exponent, calculated from the equilibrium condition. It should be noted that p_{max}, ψ_{max} and c depend on the load. Their trends for the simulated MoP implant (Tab. 2) are plotted in Fig. 6.

3.3.2. Sliding velocity

The sliding velocity is the velocity of a point P of the cup surface with respect to the corresponding contact point Q on the head. Considering the cup as fixed and neglecting the effect of the cup elastic deformation on the kinematics, the sliding velocity could be easily evaluated as the opposite of the velocity of Q

$$\boldsymbol{v}_P = -\boldsymbol{v}_Q = -\left(\boldsymbol{v}_{O_h} + \boldsymbol{\omega} \times O_hQ\right) \tag{15}$$

where O_h is the head centre and ω the head angular velocity. The position of O_h was calculated knowing the istantaneus loading direction.

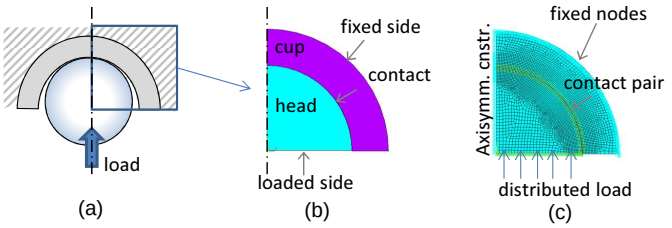

Figure 5: Hip implant simplified scheme (a). FE model scheme (b). FE mesh, with axisymmetric constraints on the axis (c).

3.3.3. Wear indicators

The proposed model evaluates the linear wear depth $h(P)$ at every point of the cup surface

$$h(P) = \int_0^T h_r(P,t)\, dt \tag{16}$$

and the volumetric wear V

$$V = \int_A h(P)\, dA \tag{17}$$

over a single gait cycle. However, since the up-date of the geometry was not implemented, the wear after n gait cycles was obtained simply by multiplying h and V by n.

4. Results

All the results presented in this section were obtained for the MoP hip implant characterized in Tab. 2, having $r_h = 14$ mm, $cl = 0.08$ mm, $t_c = 8$ mm, $\alpha = 0°$ and $\beta = 35°/45°$ for the in *in-vivo*/hip simulator BCs respectively.

Wear indicators, i.e. the linear and the volumetric wear, are referred to 10^6 cycles (1 Mc), that is approximately 1 year of activity [35]. Moreover pressure, CS_s and linear wear maps are visualized by means of 2D contour plots, projected on the $x_c - y_c$ plane. It is worth reminding that it was assumed that only the acetabular cup is subjected to wear, therefore no results are reported for the head.

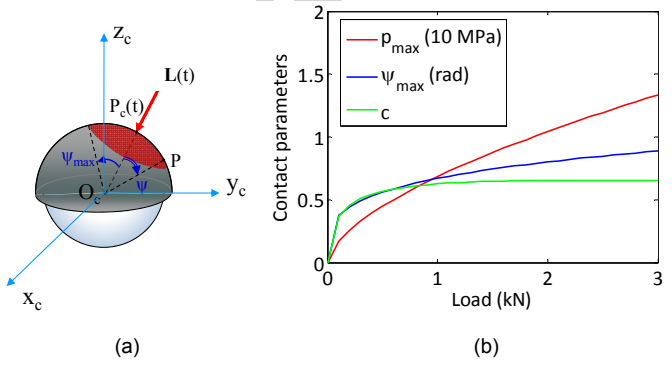

Figure 6: Contact parameters of Eq. 14: (a) schematic representation; (b) trends vs. load.

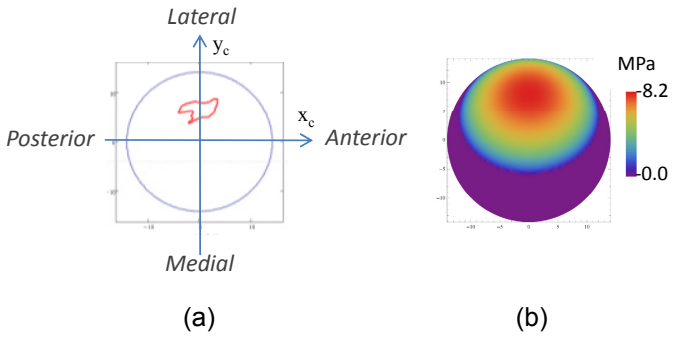

Figure 7: Trajectory of the theoretical contact point (a) and contact pressure distribution at the maximum load (b), in the cup $x_c - y_c$ plane under *in-vivo* gait conditions.

4.1. Comparison of the wear laws

The comparison of the wear laws in Table 1 was carried out assuming *in-vivo* gait conditions, i.e. Figs. 4-c,d. In all cases, the trajectory of the theoretical contact point $P_c(t)$ and the contact pressure at the maximum load are those depicted in Figs. 7-a and b, respectively. The linear wear maps predicted by the proposed model according to different wear laws are shown in Fig. 8. All the maps are characterized by a worn area located laterally to the north pole' of the acetabular cup and extended to both the anterior and the posterior quadrants. Furthermore all the wear laws indicated a maximum wear depth nearly in the same cup region, where the trajectory of $P_c(t)$ and the maximum contact pressure occurr. A qualitative analysis of Fig. 8 also points out that similar wear maps are predicted by the models based on the Archard's wear law, though varying the wear factor expression, whilst a different wear distribution was obtained using the new wear law, (i.e. Eq.11). Indeed in the latter case the maximum linear wear affected a wider area. On the other hand, significant differences arise from a quantitative examination of results shown in Fig. 8: both the linear and the volumetric wear are strongly affected by the particular wear factor/coefficient used. The resulting maximum wear depth and the volumetric wear varied in wide ranges, 0.035–0.158 mm and 12–37 mm^3 respectively, both assuming the highest value for $k_f(R_a)$ and the lowest value for $k_c(CS_r)$.

4.2. Effect of the kinematic conditions

The effect of the kinematic conditions on wear was investigated by comparing the wear predictions associated to three different motion types, characterized by one, two and three non-zero angular velocity components (Figs. 4 b), respectively. In particular the former case simulates a simple flexion-extension motion, assuming only ω_y different from zero; the second one, labelled $\omega_y - \omega_z$, add the internal-external rotation about the z-axis while the latter case, with full gait three-dimensional vector, is denoted as $\omega_x - \omega_y - \omega_z$. Additionally, for each velocity component, the temporal trend of *in-vivo* gait cycle (Fig. 4 d) was assumed. Each kinematic condition caused different sliding velocities and therefore also different CS_s. For the three cases, the obtained average CS_s was 0.172, 0.034 and 0 decreasing with the number of (non-zero) angular velocity com-

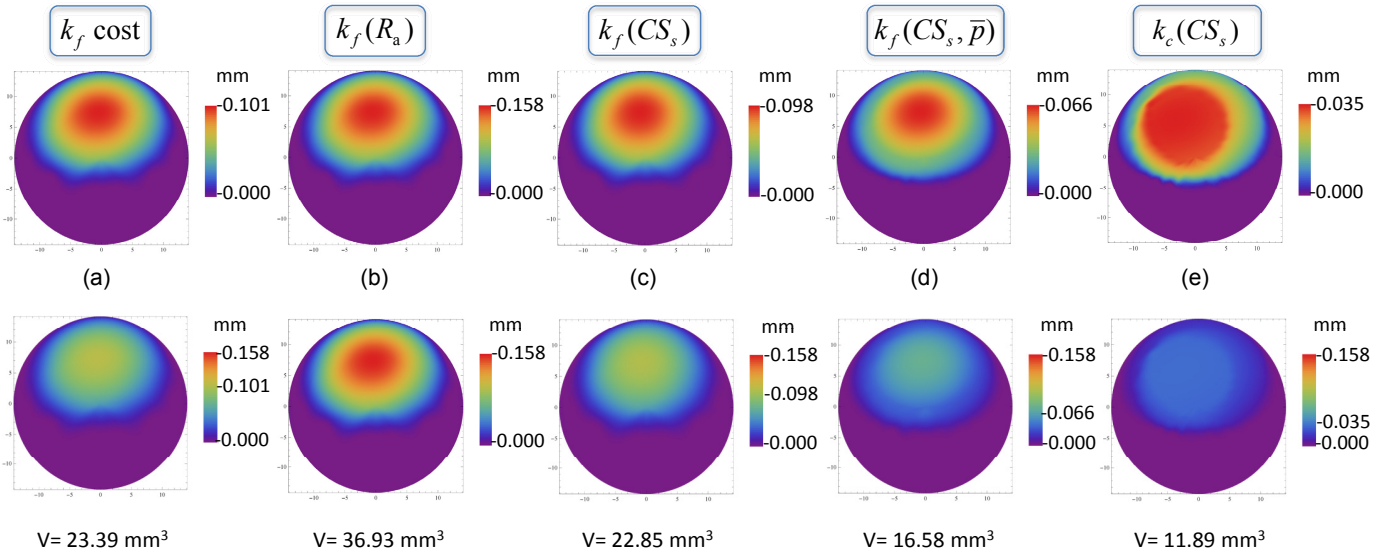

Figure 8: Acetabular cup linear wear maps (in the $x_c - y_c$ plane) and volumetric wear after 1 Mc, predicted using different wear laws, under *in-vivo* gait conditions. In the first row each plot is represented within its own minimum and maximum values, while in second row the same range is used for all plots to ease their comparison.

ponents. Indeed under the only flexion-extension movement the sliding velocity had a constant direction and hence $CS_s = 0$. Figures 9-a,b show the CS_s maps for the other two cases, which appear significantly different. In fact, in the full 3D condition (Fig. 9-a) the central region of the worn area (close to $x_c = 0$) is characterized by high values of CS_s, whilst its posterior/anterior edges by low ones. An opposite trend can be observed for the $\omega_y - \omega_z$ condition: Fig. 9-b clearly shows an almost zero CS_s for the contact points close to $x_c = 0$, which in fact have nearly uni-directional trajectories. The wear indicators obtained with the three cases are summarized in Fig. 10, showing the influence of the kinematic conditions: the more complicated and realistic the angular velocity, the higher CS_s and the higher the linear and the volumetric wear rates. The wear depths varied with the wear law confirming trends observed in Sec. 4.1: the highest and the lowest wear depths were obtained for $k_f(R_a)$ and $k_c(CS_s)$, respectively. As shown in Fig.10-c, the percentage difference of V and h_{max} between complete 3D and simple flexion-extension movement ranged between 16 – 44% and 17 – 45%, respectively. This percentage variation highlighted the higher sensitivity of the model based on $k_f(CS_s)$ to the kinematic conditions, which is significantly reduced when also the mean pressure is taken into account in $k_f(CS_s, \bar{p})$.

4.3. Effect of the loading conditions

The effect of the loading conditions was investigated in two directions: on the one hand as effect of one or more load components and the on the other hand as influence of the load level, which is related to the Body Weight (BW). In both cases, the kinematic conditions were those of the 3D *in-vivo* gait (Fig. 4-d), therefore the CS_s map corresponds to Fig. 9-a.

In analogy with the previous section, the action of L_z alone or combined with the other load components (Fig. 4-a) was considered, assuming the trends of the *in-vivo* gait cycle in Fig. 4-c. Since the vertical component (L_z) is much higher than the other ones, the simulations produced very similar results, corresponding to those reported in Sec.4.1. It is worth noting that the presence of time-varying components gives a variable load direction and therefore a curve of nominal contact points on the cup (Fig. 7-a); on the other side a single component entails a fixed contact point.

Then, the effect of the Body Weight was investigated by comparing the wear induced by three different loads levels obtained scaling the *in-vivo* load in Fig. 4-c of 80-100-120%. The resulting wear indicators are reported in Fig. 11. It can be observed that all models based on the Archard wear law show a rather linear variation of both the linear and the volumetric wear with load. Differently, assuming the new wear law, the volumetric wear slightly increases by increasing the load, although the linear wear depth remains unchanged. In particular, a load increase (decrease) by 20% induces differences in h_{max} and V of 0 – 13% (-15 – 0.6%) and 9 – 21% (-20 – -9%) as detailed in Fig. 11-c, respectively. The variation of the wear indicators according to the wear law was in agreement with those of Figs. 8 and 10: the highest h and V values were obtained for $k_f(R_a)$ and the lowest ones for $k_c(CS_s)$.

4.4. Comparison of the wear predicted under in-vivo and hip simulator conditions

The combined effect of the kinematic and the loading conditions on wear was finally investigated, comparing the *in-vivo* and the hip simulator boundary conditions, reported in Figs. 4-c,d and Figs. 4-e,f respectively.

First of all it is worth noting that the two conditions caused different contact pressures and CS_s values. The contact pressure due to simulator loading was higher up to 33% compared

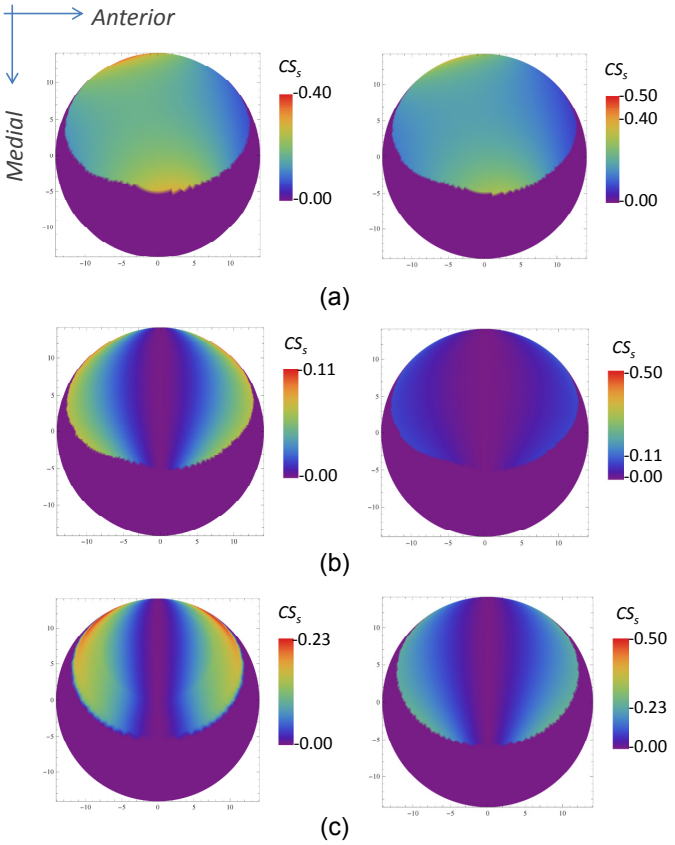

Figure 9: CS_s maps for three different kinematics conditions: complete *in-vivo* gait velocity (a), simplified case with ω_y–ω_z (b), Leeds ProSim simulator (c). In the left column each plot is represented within its own minimum and maximum values while in the right column all the CS plots are depicted in the same range (0–0.5).

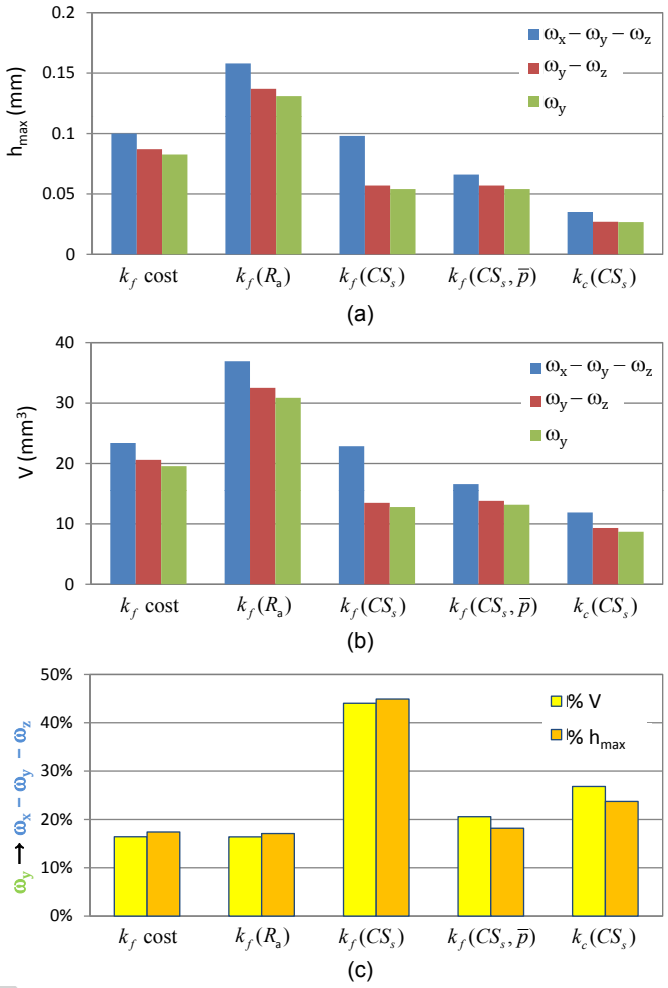

Figure 10: Effect of the kinematic conditions on the linear (a) and the volumetric (b) wear after 1 Mc. Percentage volumetric wear variation between a full 3D and a flexion-extension motion (c).

to the *in-vivo* conditions. The average CS_s value under simulator BCs was 0.088, lower (-50%) than the *in-vivo* one. The CS_s maps for the two cases are shown Figs. 9-a,c for the *in-vivo* and hip simulator kinematics, respectively. For the latter, the CS_s lowest values were predicted close to the x_c axis, whilst the highest ones in the posterior and anterior edges of the worn area. The map was similar to that one of $\omega_y - \omega_z$ case (Fig. 9-b), which indeed accounted for the same motion components of the simulator.

As fas as wear results are concerned, different wear maps were predicted for the two cases. As an example, those obtained both for the Archard wear law with $k_f(CS_s, \bar{p})$ and for the new wear law are compared in Fig. 12. It can be observed that both BCs gave similar maps when the Archard's wear law was used (Fig. 8-d vs. Fig. 12-a), although with different maximum values (0.066 mm vs. 0.055 mm), higher for the *in-vivo* case. On the contrary the new wear law produced rather different maps (Fig. 8-e vs. Fig. 12-b) and maximum wear depth for the simulator condition (0.035 mm vs. 0.037 mm). A comparison of the maximum linear wear and the volumetric wear under the *in-vivo* and the simulator BCs for all wear models is proposed in Fig. 13: both the wear indicators resulted lower under simulator BCs, with the exception of h_{max} calculated assuming $k_c(CS_s)$, as commented above.

5. Discussion

The comparison of the most recent wear laws for SoH hip implants, implemented in the proposed wear model, underlined a remarkable variability of the results with the wear factor/coefficient. The sensitivity of the wear laws to the kinematic and the loading conditions is discussed in the following sections. Some general remarks on CS ratio definition and evaluation are also reported.

5.1. *Effect of the kinematic conditions*

The kinematic conditions affect the wear law through both the sliding velocity and the CS_s. Accordingly, our results were influenced by the kinematic conditions, especially those obtained with wear laws dependent on the CS_s. In particular, it was observed that the more complicated the kinematic conditions, the higher the CS_s and the wear factor/coefficient, the higher the wear indicators, (the variations of h_{max} and V were similar). Indeed, as shown in Fig. 10, the full gait motion caused higher V and h_{max} than the simplified flexion-extension one and their percentage differences were maximum

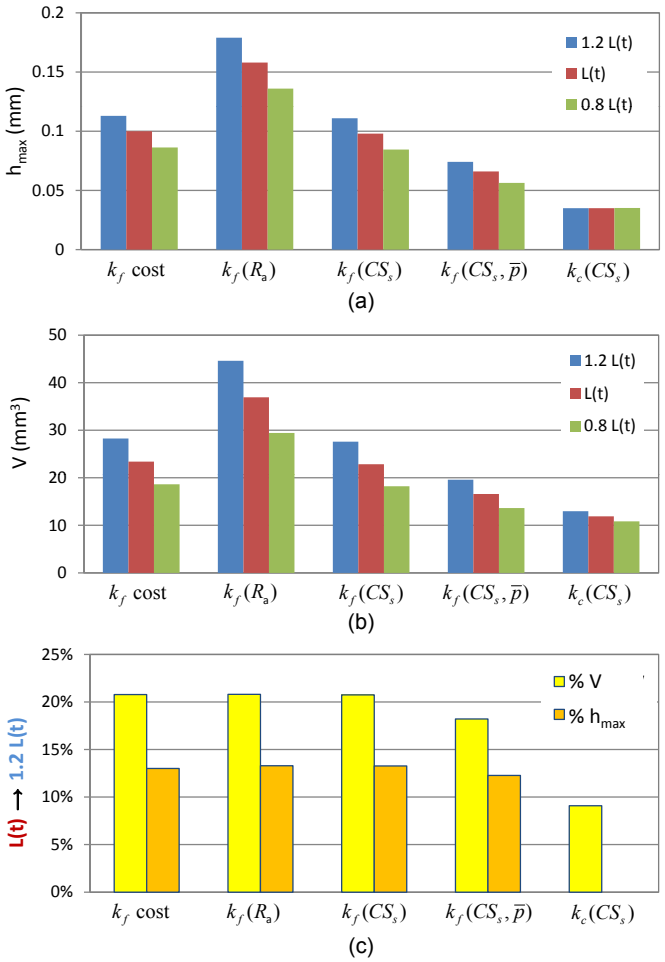

Figure 11: Effect of the Body Weight on the linear (a) and the volumetric (b) wear after 1 Mc. Percentage difference of the volumetric wear caused by a 20% increase of the *in-vivo* load (c).

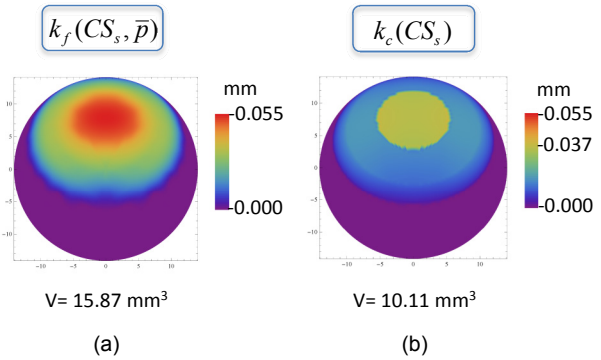

Figure 12: Linear wear maps (in the $x_c - y_c$ plane) and volumetric wear after 1 Mc, predicted assuming two different wear laws, under Leeds ProSim simulator BCs. Plot are represented in the same range of values, however the maximum wear depth in (b) was 0.037 mm).

for $k_f(CS_s)$ and $k_c(CS_s)$. In the case of $k_f(CS_s,\bar{p})$ the effect of a higher CS_s was like to be balanced by the high $\bar{p}$ (the higher $\bar{p}$ the lower $k_f(CS_s,\bar{p})$), yielding to lower $k_f(CS_s,\bar{p})$ and thus to lower wear rates. The obtained results were in agreement with the literature. Indeed the influence of the kinematics on wear, often referred to as the effect of multi-directional sliding, has been demonstrated in numerous experimental studies. A variation in the slide track shape was shown to cause a huge variation in the wear rate in *in-vitro* studies carried out both on hip simulators [36] and on pin-on-disk devices [37]. On the other hand in [38] positive correlations were found between the wear rate measured *in-vivo* by radiography and the product of the average sliding distance and the inverse of the average aspect ratio of the loci of the contact points, obtained from patient gait analysis. Moving of these observations, the modelling of the CS effect, which enhances the effect of the kinematics on the wear, appears fundamental in order to obtain more reliable wear predictions.

5.2. *Effect of the loading conditions*

Our model also allowed to investigate how the wear of hip implants is affected by the loading conditions and by the patient's body weight. Results indicated that, for the *in-vivo* condition, a three-dimensional load produced similar wear as the uniaxial vertical one, for all the wear laws. Moreover a scale factor on the load induced a rather proportional wear volume and wear depth when the Archard wear law was considered; on the other hand, the new wear law predicted a V variation approximately half the load variation while the wear depth remained almost unchanged. Consequently, it can be affirmed that the two wear laws exhibited a different response to the load level. In fact the load affects the wear through the contact pressure and the contact area in the Archard wear law, but only through the contact area in the new wear law. This result suggested the new wear law as the most suitable one for describing the effect of the load on wear. Indeed experimental investigations have demonstrated a poor correlation between load and wear, in terms of both loading components and law. As an example, similar wear rates wear predicted by hip simulators adopting a 3D load [39] versus a vertical load [40]. Other studies confirmed that simplified loading cycles produced wear rates similar to the physiological ones [41, 42]. As far as the loading conditions is concerned, the only aspect which might affect the wear is the velocity of the load application. The hip simulator study presented in [43] reported that, for plastic cup with high R_a ($\approx$ 0.3 μm), an increase in load speed led to a massive increase in wear.

Actually, the effect of the activity level on the wear still remains an open issue. The exposure of hip joints to a greater number of walking cycles or different activities should theoretically contribute to variation in the long-term wear performance of their replacements [44]. Nevertheless experimental studies showed no relationship between wear and patient activity levels [45–47]. Unfortunately, nowadays numerical investigations on this aspect cannot be carried out since they would require k_f and k_c being evaluated under a dynamic pressure rather than a constant one.

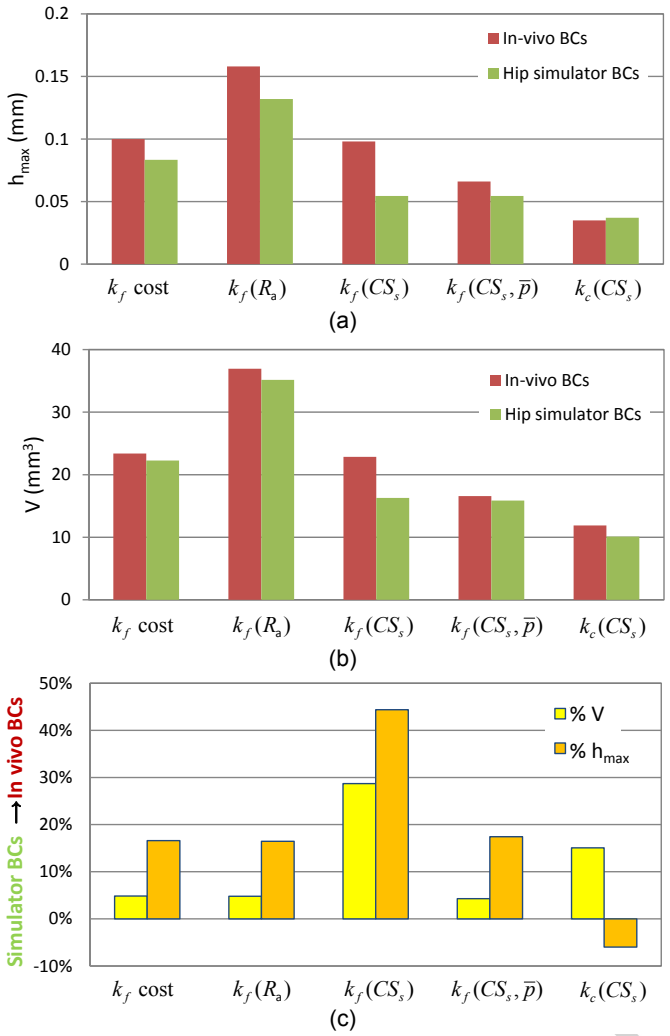

Figure 13: Effect of the boundary conditions on the linear (a) and the volumetric (b) wear after 1 Mc and percentage difference of the volumetric wear (c).

5.3. *Comparison of the wear predicted under in-vivo and hip simulator conditions*

Wear simulations are often carried out by means of experimental tests in hip simulators, which implement simplified kinematic and loading gait conditions. Our results support the necessity to design hip simulators that reproduce physiological gait conditions as much as possible especially in terms of kinematics, whilst a simplification can be tolerated on the loading components and magnitude, which is in agreement with [48, 42, 41]. In particular our results indicated that under simulator conditions the wear rates were underestimated with respect to the *in-vivo* conditions. The underestimations of V and h_{max} varied with the wear law, however being quite high, up to 28% and 44%, respectively. Nevertheless it should be considered that many different hip simulators are actually used to test wear of hip implants. As reviewed by Calonius and Saikko [48], such simulators apply different kinematics which generate different slide tracks and likely cause different wear.

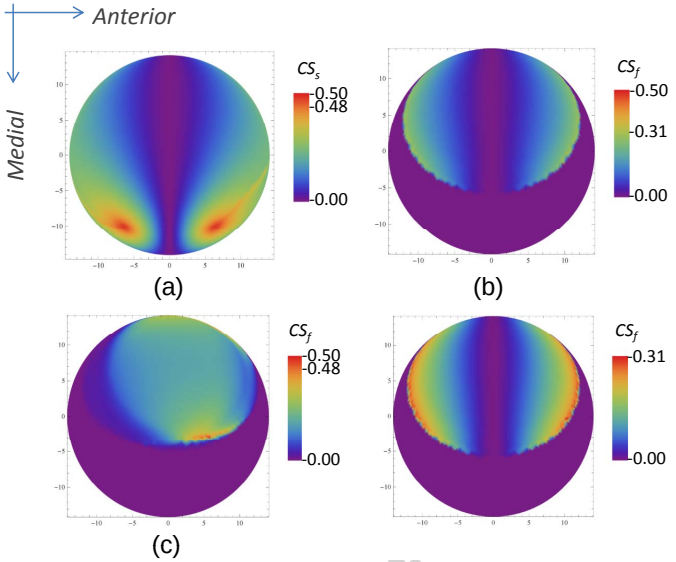

Figure 14: Maps obtained according to different CS definitions: CS_s calculated by replacing the sliding velocity with the relative velocity, under Leeds ProSim simulator (a); CS_f under Leeds ProSim simulator (b) and *in-vivo* (c) BCs. Case (b) is plotted twice: in the full CS range (above) and within its own range (below). For cases (a) and (c) the two ranges were similar, as the maximum value was 0.48 for both.

5.4. *Remarks on the definition and the calculation of the CS ratios*

The cross-shear effect is surely a fundamental aspect of the wear of SoH bearings, but unfortunately there are still some open issues on its modelling. According to Eq. (8), the CS_s can be defined only for contact points where the sliding velocity is non-zero during the whole gait cycle (otherwise Eq. (8) would yield to an indeterminate case). However in some studies, as [23, 26], the CS_s is evaluated all over the cup surface without considering where the contact actually occurs, as if the relative velocity was used instead of the sliding velocity in Eq. (8). An example of the CS_s map obtained with the relative velocity for hip simulator BCs is reported in Fig. 14-a: the maximum CS_s ratios were localized in the medial cup, outside the contact area, in agreement with the findings in [23]. Obviously the CS_s maps evaluated according to the simplified and the full definition (Fig. 9-c) matched were the contact occurred.

Another critical point regards the use of the simplified form of the CS_r (Eq. (8)), in particular the replacement of the istantaneous pressure with its average value. In order to verify the validity of this assumption, some simulations were carried out calculating the CS_f according to Eq. (7). As an example, the maps of CS_f obtained under hip simulator and *in-vivo* BCs are shown in Figs. 14-b,c, respectively, which differ from the correspondent CS_s ones shown in Figs. 9-c,a. Such difference is more evident in the case of *in-vivo* BCs since the area with non-zero CS_f appears like moved towards the anterior direction with respect to the CS_s map. The average (maximum) values of cross-shear ratio comparing CS_f vs. CS_s gave 0.09 vs. 0.1 (0.31 vs 0.23) and 0.17 vs. 0.15 (0.48 vs. 0.4) for hip simulator and *in-vivo* BCs, respectively. However, despite such differences, rather negligible variations were observed in the wear

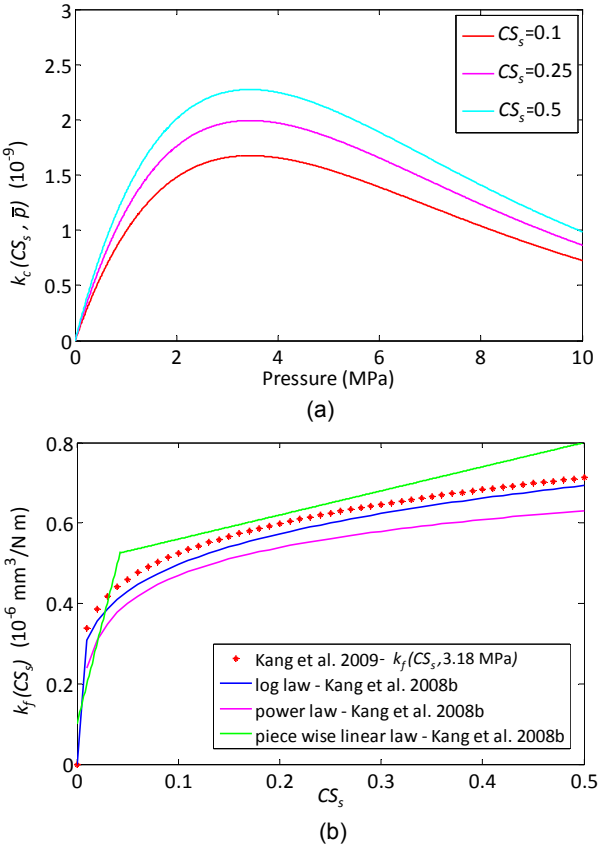

Figure 15: Wear coefficient calculated as $k_f(CS_s, \bar{p})\bar{p}$, with $k_f(CS_s, \bar{p})$ taken from [24] (a). Comparison of different fittings of the same data set of $k_f(CS_s)$, evaluated at a pressure of 3.18 MPa (b).

indicators, e.g. the percentage difference of V and h_{max} ranged between 0 – 2%. Consequently, also considering the higher computational cost of the CS_f calculation with respect to CS_s, the CS_s can be considered an acceptable semplification.

It should be noted also that the use of the correct definition of the CS_r in the new wear law would cause the wear rate to be explicitly dependent on the contact pressure, which is in disagreement with the law itself, formulated *ad hoc* for eliminating such dependence. A further clarification is needed as far as the new wear law is concerned. The expression of k_c proposed by Liu et al. [26] (Eq. (13)) was obtained from the k_f defined in [30] according to $k_c(CS_s) = k_f\ (CS_s)\ \bar{p}$, where $\bar{p}$ is the constant pressure used in the wear test. Additionally Liu et al. [26] considered k_c almost constant under the pressures of interest, although a significant variation is showed in their study, particularly in the range 1 – 6 MPa. Indeed the calculation of k_c as $k_c(CS_s, \bar{p}) = k_f(CS_s, \bar{p})\bar{p}$, exploiting data set from [24], would yield to the dependence of k_c with the pressure plotted in Fig. 15-a.

Another questionable point concerns the analytical expressions of $k_f(CS_s)$, $k_f(CS_s, \bar{p})$ and $k_c(CS_s)$ obtained by pin on plate wear tests under constant pressures. Firstly, the experimental test campaign was quite limited and a scant number of data was used for extrapolating k_f and k_c curves. Thus the fitting of the same data set by different functions yielded to rather different trends, as depicted in Fig. 15-b.

In addition sometimes the analytical expressions are not valid throughout the domain of CS_s: e.g. in case of unidirectional motion (i.e. $CS_s = 0$) $k_f(CS_s)$ provides an unreasonable value of the wear factor whilst $k_f(CS_s, \bar{p})$ predicts no wear. In order to avoid this, a minimum CS_s value equal to 0.06 was employed in the evaluation of the wear factor/coefficient. Finally the effect of a dynamic pressure on the wear factor/coefficient was neglected even if it is recognized to strongly affect the wear of UHMWPE [49].

Beyond the limitations discussed thus far, a recent study by Lee et al. [50] has highlighted the necessity of a better understanding of the CS effect. In their attempt to clarify some inconsistencies between theoretical and experimental findings, Lee et al. [50] revised the CS_s definition previously proposed by the same group (Eq. (3)). They basically observed that the frictional work released in the PMO and the CS direction, concurred both to molecular reorientation and to wear. However Lee et al. [50] suggest not to extrapolate their conclusions and consequently their indications were not included in the proposed wear model.

Finally, other wear models of the cross-shear effect are worth mentioning, as the one proposed by Hamilton et al. [51] for total knee replacement and the more recent one by Dressler et al. [52], which takes into account the crossing motion history and the actual path scale. Such models were not considered in this study as they were not yet applied to hip replacements and this would require specific validation tests.

5.5. Comparison with predicted and clinical wear estimations

The current model was developed with the aim of comparing the most recent wear laws for the UHMWPE acetabular components. Indeed such laws were implemented in models with different characteristics (e.g. geometries, material properties or BCs) and hence not directly comparable. For the same reason the comparison of our results with other numerical wear rates can be only qualitative and it is certainly even harder with respect to clinical wear rates, typically highly dispersed. Nevertheless, on completion of the discussion section, a comparison with the literature is provided in the following.

As far as the numerical wear predictions is concerned, slightly lower wear rates were predicted by our model. Raimondi et al. [16] investigated an implant with a higher clearance (cl=0.1 mm vs. cl=0.08 mm) and obtained V=70 mm^3/Mc and about h_{max}=0.85 mm/Mc under *in-vivo* loading conditions from [53] with BW 70 kg and kinematic conditions from [54]. Kang et al. [23], for an implant with same radius as our but clearance not specified, predicted V=26.7 mm^3/Mc and h_{max}=0.07 mm/Mc under Leeds ProSim hip simulator BCs (k_f for average pressure of 1 MPa and for 0 MRad polyethylene, according to Table 1). Kang et al. [24] estimated V=13 mm^3/Mc and h_{max}=0.035 mm/Mc for an MoP implant similar to [16], under Leeds ProSim hip simulator BCs. It is worth noting that the contact pressure was calculated according to the hertzian theory in [16] and to the constrained column model in [23, 24]. Liu et al. [26] assumed an MoP implant with the same geometry of the proposed one, under Leeds ProSim hip simulator BCs

with a modified loading cycle [55], obtaining V=23 mm^3/Mc and about h_{max}=0.042 mm/Mc. Their model, differently from the other ones, considered an elastic-plastic behavior for the plastic cup.

The current wear model, as the above mentioned ones, underestimates clinical wear measured both *in-vivo* and *ex-vivo*.

For instance, Kabo et al. [4] evaluated an average V rate of 75.6mm ^{3}/Mc and average linear wear rates of 0.234 mm/Mc for implants with r_h = 14 mm. Livermore et al. [3] reported a volumetric wear rate in the range 0 – 225 mm^3/Mc (average value of 48.4 mm^3/Mc) and linear wear rates in the range 0 – 0.3 mm/Mc (average value of 0.08 mm/Mc). More recently, much higher wear rates were measured by Chuter et al. [10] of about 105 – 430 mm^3/Mc (average value of 227 mm^3/Mc) and 0.21 – 0.66 mm/Mc (average value of 0.45 mm/Mc). However it should be considered that a comparison with clinical data is very difficult because of their high dispersion mainly due to dependence of *in-vivo* wear on many factors (e.g. BW, age, lifestyle/daily activities, PE oxidation and aging). Moreover it has been demonstrated that the wear measurements can also be affected on the experimental method exploited [10].

However the deviation between our results and numerical/clinical wear rates reported in the literature was expected as a consequence of the model simplifying hypotheses which were necessary for the development of a numerical tool with a low computational cost.

6. Conclusion

An advanced mathematical wear model for SoH hip implants was developed. Several aspects were improved with respect to the previous mathematical wear model by Raimondi et al. [16]), among which: the contact pressure, calculated by FE analysis instead of Hertzian theory; the sliding distance, evaluated more precisely by applying the kinematic law rather than by summing circumference arches; the wear law, since the present model implemented the most recent wear laws including the cross-shear effect. The parametric formulation and the low computational cost of our model were exploited to carry out a numerical comparison of such wear laws and to investigate their sensitivity to loading and kinematic conditions. All the simulations highlighted the remarkable variability of results with the wear law/factor. To give an example, under *in-vivo* gait conditions, percentage differences of h_{max} and V up to 210% and 350% respectively, were obtained (Fig. 8). As a general trend, the highest wear was predicted by $k_f(R_a)$; similar wear rates were obtained for constant k_f and $k_f(CS_s)$, whilst the lowest wear rates were for $k_f(CS_s, \bar{p})$ and $k_c(CS_s)$. In terms of relative variations, the wear model based on the $k_f(CS_s)$ resulted the most sensitive to the kinematic and loading conditions. The fundamental role of the wear law/factor in the reliability of the wear model was highlighted, as well as some critical aspects of the examined laws. Ongoing research will address the improvement of the model by implementing the up-date of the geometry due to wear and by evaluating the component of the sliding velocity due to cup elastic deformation.

[1] Nayak, N.K., Mulliken, B., Rorabeck, C.H., Bourne, R.B., Robinson, E.J.. Osteolysis in cemented versus cementless acetabular components. The Journal of Arthroplasty 1996;11(2):135–140.

[2] Ma, T., Goodman, S.B.. 6.606 - biological effects of wear debris from joint arthroplasties. In: Comprehensive Biomaterials; vol. 6. Oxford: Elsevier; 2011, p. 79–87.

[3] Livermore, J., Ilstrup, D., Morrey, B.. Effect of femoral head size on wear of the polyethylene acetabular component. Journal of bone and Joint Surgery 1990;72(4):518–28.

[4] Kabo, J., Gebhard, J., Loren, G., Amstutz, H.. In vivo wear of polyethylene acetabular components. J Bone Joint Surg Br 1993;75-B(2):254–258.

[5] McCalden, R.W., Naudie, D.D., Yuan, X., Bourne, R.B.. Radiographic methods for the assessment of polyethylene wear after total hip arthroplasty. Journal of bone and joint surgery 2005;87(10):2323–34.

[6] Hall, R.M., Unsworth, A., Siney, P., Wroblewski, B.M.. Wear in retrieved charnley acetabular sockets. Proceedings of the Institution of Mechanical Engineers, Part H: Journal of Engineering in Medicine 1996;210(3):197–207.

[7] Sychterz, C., Moon, K., Hashimoto, Y., Terefenko, K., Anderson, C., Bauer, T.. Wear of polyethylene cups in total hip arthroplasty. Journal of Bone and Joint Surgery 1996;78(8):1193–2000.

[8] Jasty, M., Devon, G., Bragdon, C.R., Lee, K.R., Hanson, A.E., Elder, J.R., et al. Wear of polyethylene acetabular components in total hip arthroplasty. an analysis of one hundred and twenty-eight components retrieved at autopsy or revision operations. Journal of bone and joint surgery 1997;79:349–58.

[9] Elfick, A.P.D., Hall, R.M., Pinder, I.M., Unsworth, A.. Wear in retrieved acetabular components: Effect of femoral head radius and patient parameters. The Journal of Arthroplasty 1998;13(3):291–295.

[10] Chuter, G.S.J., Cloke, D.J., Mahomed, A., Partington, P.F., Green, S.M.. Wear analysis of failed acetabular polyethylene: A comparison of analytical methods. Journal of Bone and Joint Surgery - British Volume 2007;89-B(2):273–279.

[11] Saikko, V.. A multidirectional motion pin-on-disk wear test method for prosthetic joint materials. Journal of Biomedical Materials Research 1998;41(1):58–64.

[12] Kaddick, C., Wimmer, M.A.. Hip simulator wear testing according to the newly introduced standard iso 14242. Proceedings of the Institution of Mechanical Engineers, Part H: Journal of Engineering in Medicine 2001;215(5):429–442.

[13] Mattei, L., Di Puccio, F., Piccigallo, B., Ciulli, E.. Lubrication and wear modelling of artificial hip joints: a review. Tribology International 2011;44:532549.

[14] Maxian, T.A., Brown, T.D., Pedersen, D.R., Callaghan, J.J.. A sliding-distance-coupled finite element formulation for polyethylene wear in total hip arthroplasty. Journal of Biomechanics 1996;29(5):687–692.

[15] Maxian, T., Brown, T., Pedersen, D., Callaghan, J.. 3-dimensional sliding-contact computational simulation of total hip wear. Clinical orthopaedics and related research 1996;333:41–50.

[16] Raimondi, M.T., Santambrogio, C., Pietrabissa, R., Raffelini, F., Molfetta, L.. Improved mathematical model of the wear of the cup articular surface in hip joint prostheses and comparison with retrieved components. Proceedings of the Institution of Mechanical Engineers; Part H; Journal of Engineering in Medicine 2001;215(4):377–91.

[17] Maxian, T., Brown, T., Pedersen, D., McKellop, H., Lu, B., Callaghan, J.. Finite element analysis of acetabular wear. validation, and fixation and backing effects. Clinical orthopaedics and related research 1997;344:111–117.

[18] Brown, T.D., Stewart, K.J., Nieman, J.C., Pedersen, D.R., Callaghan, J.J.. Local head roughening as a factor contributing to variability of total hip wear: a finite element analysis. Journal of Biomechanical Engineering 2002;124(6):691–8.

[19] Wang, A., Sun, D.C., Yau, S.S., Edwards, B., Sokol, M., Essner, A., et al. Orientation softening in the deformation and wear of ultra-high molecular weight polyethylene. Wear 1997;203-204:230–241.

[20] Turell, M., Wang, A., Bellare, A.. Quantification of the effect of cross-path motion on the wear rate of ultra-high molecular weight polyethylene. Wear 2003;255(7-12):1034–1039.

[21] Barbour, P.S.M., Barton, R.C., Fisher, N.. The influence of contact stress on the wear of uhmwpe for total replacement hip prostheses. vol. 181-183 of *Wear (Switzerland)*. Switzerland; 1995, p. 250–7.

[22] Wang, A., Essner, A., Klein, R.. Effect of contact stress on friction and wear of ultra-high molecular weight polyethylene in total hip replacement. Proceedings of the Institution of Mechanical Engineers, Part H (Journal of Engineering in Medicine) 2001;215(H2):133–9.

[23] Kang, L., Galvin, A.L., Brown, T.D., Fisher, J., Jin, Z.M.. Wear simulation of ultra-high molecular weight polyethylene hip implants by incorporating the effects of cross-shear and contact pressure. Proceedings of the Institution of Mechanical Engineers, Part H (Journal of Engineering in Medicine) 2008;222(H7):1049–64.

[24] Kang, L., Galvin, A.L., Fisher, J., Jin, Z.. Enhanced computational prediction of polyethylene wear in hip joints by incorporating cross-shear and contact pressure in additional to load and sliding distance: Effect of head diameter. Journal of Biomechanics 2009;42(7):912–918.

[25] Wang, F.C.. Microscopic asperity contact and deformation of ultra-high molecular weight polyethylene bearing surfaces. Proceedings of the Institution of Mechanical Engineers; Part H; Journal of Engineering in Medicine 2003;217(6):477–90.

[26] Liu, F., Galvin, A., Jin, Z., Fisher, J.. A new formulation for the prediction of polyethylene wear in artificial hip joints. Proceedings of the Institution of Mechanical Engineers, Part H: Journal of Engineering in Medicine 2011;225(1):16–24.

[27] Buford, A., Goswami, T.. Review of wear mechanisms in hip implants: Paper i - general. Materials & Design 2004;25(5):385–393.

[28] Streicher, R.M., Schn, R.. Tribological behaviour of various materials and surfaces against polyethylene. In: 17th Annual Meeting of the Society for biomaterials. 1991, p. 289.

[29] Wang, A., Polineni, V.K., Stark, C., Dumbleton, J.H.. Effect of femoral head surface roughness on the wear of ultrahigh molecular weight polyethylene acetabular cups. The Journal of Arthroplasty 1998;13(6):615–620.

[30] Kang, L., Galvin, A.L., Brown, T.D., Jin, Z., Fisher, J.. Quantification of the effect of cross-shear on the wear of conventional and highly cross-linked uhmwpe. Journal of Biomechanics 2008;41(2):340–346.

[31] Brockett, C., Williams, S., Jin, Z., Isaac, G., Fisher, J.. Friction of total hip replacements with different bearings and loading conditions. Journal of Biomedical Materials Research Part B: Applied Biomaterials 2007;81B(2):508–515.

[32] Willing, R., Kim, I.Y.. A holistic numerical model to predict strain hardening and damage of uhmwpe under multiple total knee replacement kinematics and experimental validation. Journal of Biomechanics 2009;42(15):2520–2527.

[33] Abdelgaied, A., Liu, F., Brockett, C., Jennings, L., Fisher, J., Jin, Z.. Computational wear prediction of artificial knee joints based on a new wear law and formulation. Journal of Biomechanics 2011;44(6):1108–1116.

[34] Bergmann, G., Graichen, F., Rohlmann, A., Verdonschot, N., van Lenthe, G.H.. Frictional heating of total hip implants, part 1: measurements in patients. Journal of Biomechanics 2001;34(4):421–428.

[35] Schmalzried, T., Dorey, F., McKellop, H.. The multifactorial nature of polyethylene wear in vivo. Journal of Bone and Joint Surgery 1998;80(8):1234–1242.

[36] Barbour, P.S.M., Stone, M.H., Fisher, J.. A hip joint simulator study using simplified loading and motion cycles generating physiological wear paths and rates. Proceedings of the Institution of Mechanical Engineers, Part H: Journal of Engineering in Medicine 1999;213(6):455–467.

[37] Saikko, V., Calonius, O., Kernen, J.. Effect of slide track shape on the wear of ultra-high molecular weight polyethylene in a pin-on-disk wear simulation of total hip prosthesis. Journal of Biomedical Materials Research Part B: Applied Biomaterials 2004;69B(2):141–148.

[38] Bennett, D., Orr, J.F., Beverland, D.E., Baker, R.. The influence of shape and sliding distance of femoral head movement loci on the wear of acetabular cups in total hip arthroplasty. Proceedings of the Institution of Mechanical Engineers, Part H: Journal of Engineering in Medicine 2002;216(6):393–402.

[39] Bigsby, R.J.A., Hardaker, C.S., Fisher, J.. Wear of ultra-high molecular weight polyethylene acetabular cups in a physiological hip joint simulator in the anatomical position using bovine serum as a lubricant. Proceedings of the Institution of Mechanical Engineers, Part H: Journal of Engineering in Medicine 1997;211(3):265–269.

[40] Besong, A.A., Bigsby, R.J.A., Barbour, P.S.M., Fisher, J.. Effect of head size and loading regime on the wear of uhmwpe acetabular cups in a hip simulator. In: Mechanical Engineering Publications, L., editor. World Tribology Congress. London; 1997, p. 732.

[41] Smith, S.L., Unsworth, A.. Simplified motion and loading compared to physiological motion and loading in a hip joint simulator. Proceedings of the Institution of Mechanical Engineers, Part H: Journal of Engineering in Medicine 2000;214(3):233–238.

[42] Elfick, A.P.D., Smith, S.L., Green, S.M., Unsworth, A.. The quantitative assessment of uhmwpe wear debris produced in hip simulator testing: the influence of head material and roughness, motion and loading. Wear 2001;249(5-6):517–527.

[43] Bowsher, J.G., Shelton, J.C.. A hip simulator study of the influence of patient activity level on the wear of crosslinked polyethylene under smooth and roughened femoral conditions. Wear 2001;250(1-12):167–179.

[44] Dowson, D.. New joints for the millennium: Wear control in total replacement hip joints. Proceedings of the Institution of Mechanical Engineers, Part H: Journal of Engineering in Medicine 2001;215(4):335–358.

[45] Bennett, D., Humphreys, L., OBrien, S., Kelly, C., Orr, J.F., Beverland, D.E.. Wear paths produced by individual hip-replacement patientsa large-scale, long-term follow-up study. Journal of Biomechanics 2008;41(11):2474–2482.

[46] Sechriest Ii, V.F., Kyle, R.F., Marek, D.J., Spates, J.D., Saleh, K.J., Kuskowski, M.. Activity level in young patients with primary total hip arthroplasty: A 5-year minimum follow-up. The Journal of Arthroplasty 2007;22(1):39–47.

[47] Goldsmith, A.A.J., Dowson, D., Wroblewski, B.M., Siney, P.D., Fleming, P.A., Lane, J.M.. The effect of activity levels of total hip arthroplasty patients on socket penetration. The Journal of Arthroplasty 2001;16(5):620–627.

[48] Calonius, O., Saikko, V.. Slide track analysis of eight contemporary hip simulator designs. Journal of Biomechanics 2002;35(11):1439–1450.

[49] Barbour, P.S.M., Barton, D.C., Fisher, J.. The influence of stress conditions on the wear of uhmwpe for total joint replacements. Journal of Materials Science: Materials in Medicine 1997;8(10):603–11.

[50] Lee, R.K., Korduba, L.A., Wang, A.. An improved theoretical model of orientation softening and cross-shear wear of ultra high molecular weight polyethylene. Wear 2011;271(9-10):2230–2233.

[51] Hamilton, M.A., Sucec, M.C., Fregly, B.J., Banks, S.A., Sawyer, W.G.. Quantifying multidirectional sliding motions in total knee replacements. Journal of Tribology - Transaction of the ASME 2005;127(2):280–6.

[52] Dressler, M.R., Strickland, M.A., Taylor, M., Render, T.D., Ernsberger, C.N.. Predicting wear of uhmwpe: Decreasing wear rate following a change in direction. Wear 2011;271:2879–83.

[53] Bergmann, G., Graichen, F., Rohlmann, A.. Hip joint loading during walking and running, measured in two patients. Journal of Biomechanics 1993;26(8):969–990.

[54] Sutherland, D., Olshen, R., Cooper, L., Woo, S.. The development of mature gait. Journal of Bone and Joint Surgery 1980;62(3):336–353.

[55] Liu, F., Leslie, I., Williams, S., Fisher, J., Jin, Z.. Development of computational wear simulation of metal-on-metal hip resurfacing replacements. Journal of Biomechanics 2008;41(3):686–694.

UNIVERSITÀ DI PISA

DIPARTIMENTO DI INGEGNERIA MECCANICA, NUCLEARE E DELLA PRODUZIONE

Pisa, October 21st 2011

Tribology International

Research Highlights

of the manuscript entitled

A comparative study of wear laws for soft-on-hard hip implants using a mathematical wear model

- A mathematical, parametric wear model for soft-on-hard hip implants was developed in Mathematica.
- The most recent UHMWPE wear laws, based on the cross-shear effect, were implemented and compared.
- Simulations highlighted the variability of wear predictions with the wear factors/laws.
- A sensitivity analysis showed that kinematic conditions affect wear more than loading ones.
- Despite some open issues on its evaluation, the main role of the cross-shear effect on wear comes out.